Radial and Local Time structure of the Saturnian Ring Current, revealed by Cassini

N. Sergis[1], C. M. Jackman[2], M.F. Thomsen[3], S. M. Krimigis[1,4], D. G. Mitchell[4], D. C. Hamilton[5], M. K. Dougherty[6], N. Krupp[7], R. J. Wilson.

[1] Office of Space Research and Technology, Academy of Athens, Athens, GR.
[2] School of Physics and Astronomy, University of Southampton, Southampton, UK.
[3] Planetary Science Institute, Tucson, Arizona, USA.
[4] Applied Physics Laboratory, Johns Hopkins University, Laurel, MD, USA.
[5] Department of Physics, University of Maryland, College Park, MD, USA.
[6] Blackett Laboratory, Imperial College London, London, UK.
[7] Max Planck Institute for Solar System Research, Goettingen, Germany.
[8] Laboratory for Atmospheric and Space Physics, University of Colorado, Boulder, CO, USA.

Abstract

We analyze particle and magnetic field data obtained between July 2004 and December 2013 in the equatorial magnetosphere of Saturn, by the Cassini spacecraft. The radial and local time distribution of the total (thermal and suprathermal) particle pressure and total plasma beta (ratio of particle to magnetic pressure) over radial distances from 5 to 16 Saturn radii (Rs=60,258 km) is presented. The average azimuthal current density J_φ and its separate components (inertial, pressure gradient and anisotropy) are computed as a function of radial distance and local time and presented as equatorial maps. We explore the relative contribution of different physical mechanisms that drive the ring current at Saturn. Results show that (a) the particle pressure is controlled by thermal plasma inside of ~8 Rs and by the hot ions beyond ~12 Rs, exhibiting strong local time asymmetry with higher pressures measured at the dusk and night sectors; (b) the plasma beta increases with radial distance and remains >1 beyond 8-10 Rs for all local times; (c) the ring current is asymmetric in local time and forms a maximum region between ~7 and ~13 Rs, with values up to 100-115 pA/m^2; (d) the ring current is inertial everywhere inside of 7 Rs, exhibits a mixed nature between 7 and 11 Rs and is pressure gradient driven beyond 11 Rs, with the exception of the noon sector where the mixed nature persists. In the dawn sector, it appears strongly pressure gradient driven for a wider range of radial distance, consistent with fast return flow of hot, tenuous magnetospheric plasma following tail reconnection.

1. Introduction

Saturn is a rapidly revolving planet (period of ~10.8 hr) with a relatively strong intrinsic magnetic field (~21000 nT on the surface near the equator) and significant internal plasma sources (e.g. planetary atmosphere, rings, Enceladus). The magnetic and particle pressure deflect the solar wind flow forming a large magnetosphere with a "nose" stand-off distance of 20-28 R_S (1 R_S=60,258 km), that holds a complex and dynamic electric current system. Part of this global system is the current that flows in the azimuthal direction around the planet, usually referred to as the "ring" current.

In such a fast rotating magnetosphere with a non-homogeneous plasma distribution, the total azimuthal current that flows very close to the equatorial plane, can be viewed as the sum of three components: i) the inertial drift of the near-corotating plasma (i.e. the inertial current), ii) the gradient of the perpendicular plasma pressure, present principally along the radial direction (i.e. the pressure gradient current) and iii) the anisotropy of the plasma pressures parallel and perpendicular to the field lines in the presence of field curvature (i.e. the anisotropy current).

The ring current plays a key role in the magnetosphere-ionosphere coupling in Saturn. Its azimuthal asymmetry is associated with the topology and strength of the field aligned currents. The dynamic interaction between these two current systems certainly affects, and could in some degree drive, the short time periodic variability, that although well observed in several magnetospheric properties, is still imperfectly understood.

The Saturnian azimuthal current is carried by magnetospheric charged particles, primarily water product ions (W+) and protons (H+), distributed in radial distances between ~8 and ~15 R_S, and characterized by an increased suprathermal (>3 keV) particle pressure, high (1-10) plasma beta (ratio of particle to magnetic pressure), and intense dynamic behavior. It was originally detected indirectly by its effect (depression) on the planetary magnetic field [*Ness et al.,* 1981, 1982; *Connerney et al.,* 1981, 1983] and directly, yet partially, measured by particle sensors [*Krimigis et al.,* 1981, 1983*; Mauk et al.,* 1985] during the Voyager 1 and 2 flybys. A magnetic "signature" of the Saturnian ring current was also present in the measurements obtained during the 1979 Pioneer-11 encounter [*Connerney et al.,* 1984; *Davis et al.,* 1990]. However, only much later, *Bunce et al.* [2003] were able to confirm that these magnetic perturbations were similar to those seen during the Voyager passes, further suggesting that the ring current must have been closer to the planet during the Pioneer-11 flyby, as a result of a more compressed magnetospheric state during this pass.

Since Cassini started orbiting Saturn in July 2004, the azimuthal current has been observed in much greater detail. *Bunce et al.* [2007] studied the Saturnian ring current using magnetic field measurements and an axisymmetric magnetic field model [*Connerney et al.,* 1983], and argued that the azimuthal current is primarily inertial. *Kellett et al.* [2010, 2011] used the same magnetic field model but also included particle data from 11 Cassini orbits. They concluded that the ring current density peaks of ~90 pA/m^2 at ~9 R_S, falls gradually (as 1/r) to below ~20 pA/m^2 at 20 R_S and does not vary significantly with local time. They also argued that the pressure gradient current is the most important component beyond 12 Rs, and that in the innermost region (inside of 6 Rs) the dominant inertial current can be significantly reduced by the pressure anisotropy current component. *Sergis et al.* [2007, 2010] and *Krimigis et al.* [2007] analyzed magnetic field, thermal plasma and energetic particle measurements, and showed that the azimuthal current density develops a maximum of 100–150 pA/m^2 between 8 and 12 R_S and drops with increasing radial distance faster than the 1/r rate previously derived. They further demonstrated that the Saturnian ring current is primarily inertial inside of ~8 R_S becoming increasingly pressure gradient driven and significantly more variable at its maximum region and beyond, especially during hot plasma injection events, when the suprathermal pressure increases and the local mass density is lower. The observed variability was attributed mainly to the energetic particle pressure contribution that was proven far more variable than initially assumed and modeled, but also to the plasma interchange instability events, commonly observed by Cassini in the region between 6 and 12 Rs [*Burch et al.,* 2005; *Hill et al.,* 2005; *Mauk et al.,* 2005; *Paranicas et al.,* 2007; *Chen et al.,* 2008; *Rymer et al.,* 2009; *Kennelly et al.,* 2013; *Thomsen et al.,* 2013, 2014].

In terms of ion composition and relative ion species contribution to the total pressure and to the ring current density, both thermal and hot plasma data [*Sergis et al,* 2009; *Thomsen et al.,* 2010] indicate that the relative contribution of the heavier W+ ion population (translated to nearly 70% O+), is most of the time greater than 50%, not surprising given that the ring current resides at the central, equatorial region of the fast rotating, disk-shaped plasma sheet.

Corroborating the results from *in-situ* Cassini data, wide-angle Energetic Neutral Atom (ENA) monitoring by the Ion and Neutral Camera (INCA) on Cassini, confirmed that the hot component of the ring current is a non-uniform structure [*Krimigis et al,* 2007; *Carbary et al.,* 2008b; *Sergis et al.,* 2009], indicating that long-term measurements can only describe its average state, particularly as certain magnetospheric properties are also longitude dependent.

In addition to studies that focus on data analyses, a variety of model simulations have also been developed to reproduce basic properties of the Saturnian magnetosphere, including the pressure and ring current distributions. *Achilleos et al.* [2010] introduced a model of force balance with thermal plasma and energetic particle measurements as input and equatorial observations as a boundary condition, to show that Saturn's magnetospheric field can be significantly modified by internal changes in hot plasma pressure. Using magnetic field and particle (thermal and hot plasma) measurements, *Brandt et al.* [2010] modeled the magnetic field perturbation along a given Cassini orbit and suggested that the asymmetric pressure contribution by energetic particles that are periodically injected inwards and subsequently drift around Saturn, could associate with the magnetic field periodicities in Saturn's magnetosphere. *Jia et al.* [2012] developed a global MHD model in which they assume a localized vortical flow structure in the southern ionosphere (70° S latitude) that rotates at roughly the rate of planetary rotation. Among other magnetospheric properties, they reproduced the equatorial current density distribution and they found that the azimuthal current density J_φ presents a clear local time asymmetry at all planetary rotation phases, being higher by a factor of ~2 on the night sector.

Soon after Cassini's arrival, it became clear that the Saturnian ring current is not the uniform, symmetric structure assumed by early magnetic field modeling, but its spatial distribution and in particular its dependence on local time has not been fully examined, largely because of incomplete spatial coverage. In this work, we utilize all available magnetic field, thermal plasma and energetic particle data from Cassini magnetometer (MAG), the Cassini Plasma Spectrometer (CAPS) and the Magnetospheric Imaging Instrument (MIMI), obtained between the beginning of the mission (July 2004) and the end of 2013 (mid 2012 for CAPS measurements), and present the radial and local time distribution of average particle pressure, total plasma beta and azimuthal current density in the Saturnian magnetosphere. The results are compared to those from previous studies and further discussed in the context of existing models and proposed interpretations.

2. Instrumentation and data selection

Since its arrival at the Saturnian system, Cassini has offered the opportunity of combined *in-situ* and remote observations. The Cassini Plasma Spectrometer (CAPS) [*Young et al.,* 2004] can measure thermal plasma properties (1 eV/e to 50 keV/e for ions and 0.6 eV to 28 keV for electrons), while the Magnetospheric Imaging Instrument (MIMI) [*Krimigis et al.,* 2004] measures energetic ions (3 keV to few MeV) and electrons (20 keV to 1 MeV). Thus, the combined CAPS and MIMI use covers essentially the full particle energy distribution (not possible with Pioneer or Voyager), offering in addition species and charge state separation.

The calculation of thermal plasma moments (ion number densities, ion temperatures and plasma bulk velocity) is based on numerical integration of the observed ion count rates, as described by *Thomsen et al.* [2010]. Due to field-of-view (FOV) pointing restrictions of the CAPS sensors, it is not always possible to produce plasma properties such as pitch angle distributions or the flow velocity vector. Therefore, the computation was performed only for times when the plasma flow direction was in the FOV of the sensor, the CAPS actuator was operating and the spacecraft was not rolling. In addition, we have included the plasma parameter set derived by forward modeling [*Wilson et al.,* 2008], which provides estimations of the parallel and the perpendicular ion temperature. The plasma properties we use are also not inconsistent with the radial profiles of plasma moments independently produced by *Livi et al.* [2014] using 1-D forward modeling.

The energetic particle pressure (E>3keV, also referred to as suprathermal) is computed using MIMI/CHEMS and LEMMS data, following the method described in *Sergis et al.* [2009]. The adopted time resolution for the computed suprathermal pressures is 10 minutes. This resolution ensures both reliable statistics, given the typical count rates in the region of interest, and detailed spatial coverage (Cassini can be taken as almost stationary in global scale within each 10-min interval). The magnetic field vector is measured by Cassini's fluxgate magnetometer [*Dougherty et al.,* 2004] and 10-minute averages were used as well. For the present study we combine particle data and magnetic field measurements for radial distances between 5 and 16 R_S and within ±1 Rs from the equatorial plane, as explained below.

As shown by several studies [*Krimigis et al.,* 2007; *Arridge et al.,* 2008, 2011; *Carbary et al.,* 2008a, 2015; *Sergis et al.,* 2011] the Saturnian plasma sheet is pushed away from the rotational equator, as the solar wind attack angle changes seasonally, reaching ±26.7º at solstices. As a result, measurements taken near the equatorial (rotational) plane do not always correspond to current sheet plasma environment, but can at times include also the outer (in terms of vertical distance) parts of the plasma sheet, depending on the radial distance and the seasonal and rotational phases. According to *Arridge et al.* [2011], for a radial distance of 15 Rs, the center of the plasma sheet can at times be vertically displaced by ~2 Rs, which is comparable to the typical scale heights of its ion populations [*Sergis et al.,* 2011]. In general, beyond a radial distance of ~12 Rs, the risk of miscalculating (overestimating) the radial pressure gradient becomes significant.

Fortunately, increased spatial coverage and nearly continuous measurements by the Cassini MAG and MIMI sensors, allow us to filter the hot plasma data so that intervals for which the magnetic field vector indicates that Cassini is not truly in the central plasma sheet are not included in the analysis. After several tests, we decided to consider only intervals during which the radial component of the magnetic field has an absolute value below 0.5 nT ($|Br|<0.5$ nT) and at the same time is less than one fifth of the total magnetic field $Br<0.2|B|$. These two criteria guarantee that Cassini is inside the central region of the plasma sheet without reducing significantly our sampling. The above selection process was not applied to thermal plasma moments due to their sparse distribution. Instead, CAPS data was binned in radial distance with a step of 1 Rs, and the upper (3rd) quartile of the computed thermal pressure values for each radial bin was used in our analysis, in order to minimize the risk of including measurements that correspond to the outer (uppermost/lowermost) plasma sheet. As the thermal plasma (and W^+ ions in particular) are well confined vertically [*Sergis et al.* 2011], the risk of including in our analysis high pressure intervals that do not correspond to the central plasma sheet is very limited. Since the dominant variation in plasma parameters is radial, the 1 Rs bin size is the largest we can adopt without introducing a significant systematic error. The described selection criteria ensure that our sampling is at all times confined to the central plasma sheet, suppressing errors associated with the change of the rotational or seasonal phase.

Expanding previous studies, we also include H_2+ ions (in addition to H+ and W+) for both thermal and hot plasma in the computation of the total particle pressure and the corresponding ring current component.

To investigate the dependence of particle properties on local time, we organize our analysis in four, 6-hr wide local time (hereafter LT) sectors: night, dawn, day and dusk, centered at 0000 hr, 0600 hr, 1200 hr and 1800 hr respectively, and all results are presented and discussed in that context. To test how the selected LT bin size affects the results, we repeated the same analysis for a more detailed local time binning (eight 3-hr sectors). The results and the scientific conclusions did not change notably. The distribution of the filtered measurements in radial distance and local time is shown in Figure 1. The sampling is not uniform, especially in local time, with the dawn sector less covered by all instruments. However, due to the long (nearly 10-year) period of observation, the statistical uncertainty is still significantly reduced compared to previous studies and generally lower than the intrinsic dynamics of the system for most magnetospheric regions, as the study of individual Cassini passes has shown.

3. Results

3.1 Particle pressure and plasma beta

The radial profiles for the thermal (in black), suprathermal (in red) and total (in blue) particle pressure components are shown in Figure 2 for each 6-hr LT sector (night, dawn, day, dusk) of the equatorial magnetosphere of Saturn. It is evident that for all local times thermal plasma pressure dominates at the inner part of the region under study (inside of ~7-8 Rs). With increasing radial distance, the hot particle pressure gradually becomes the major component, in spite of its variability reflected in the larger error bars. The radial distance beyond which the hot plasma pressure overrides the thermal plasma pressure varies between ~8.5 Rs at dusk and night side, and ~11.5 Rs at dawn and dayside. The total pressure is ~50% higher at dusk and night sectors with sample values at 8 Rs ~0.3 nPa at dusk and the night side (1500 to 0300) compared to ~0.2 nPa at dawn and the dayside (0300 to 1500). Thermal plasma pressure drops with radial distance, while suprathermal pressure develops a maximum region between ~7 and ~11 Rs which is much broader, and thus less clear, on the dayside. We should note that these radial profiles correspond to the average conditions of the central plasma sheet region. The fast (order of few minutes) temporal variability that has been reported, especially for the energetic particle population [*Krupp et al.*, 2005; *Krimigis et al.*, 2007], can only be reflected in the error bars. The total particle pressure P was fitted for each LT sector using polynomial functions of the form $\log P = a_0 + a_1 r + a_2 r^2 + a_3 r^3 + a_4 r^4$. The values for the a_i coefficients are given in Table 1.

In Figure 3 we present the radial profile of the total plasma beta as measured for each LT sector. The line colors adopted in Figure 3 (i.e. black for the night side, green for dawn, red for the dayside and blue for dusk) will be used throughout this study. The plasma beta becomes greater than 1 beyond 8 Rs for the dusk and night sectors, beyond 8.5 Rs for the dawn sector and outside 10 Rs for the dayside. With increasing radial distance, the plasma beta values remain generally between 5 and 10 for dusk, night and dawn sectors, and between 1 and 5 for the dayside. Towards the inner magnetosphere, as the magnetic field increases with radial distance as approximately r^3, the plasma beta drops fast, becoming <0.1 at 5 Rs for all local times. A high beta regime of the Saturnian magnetosphere, with $\beta>1$ for radial distances between 10 and 15 Rs, has been previously reported [*Sittler et al.*, 2008; *Sergis et al.*, 2009; *Thomsen et al.*; 2010]. However, none of these studies used the spatial resolution and the particle energy range we employ here. As the combined use of CAPS and MIMI data offers wide energy coverage (few eV to few MeV) for the 3 most important (in terms of pressure contribution) ion species (i.e. H+, W+ and H_2+), the plasma beta profiles presented in this study can be viewed as the most characteristic of the Saturnian magnetosphere to date.

3.2 Radial force balance and azimuthal current

Following the formulation previously used by *Sergis et al.* [2010] and *Kellett et al.* [2011], and assuming that all ion components have the same bulk velocity, we express the radial, steady-state force balance equation in the equatorial plane as:

$$\rho \frac{V_\phi^2}{r} - \frac{\partial P}{\partial r} - \frac{P_\perp}{R_C}\left(\frac{A-1}{A}\right) \approx J_\phi B_z \qquad (1)$$

where ρ is the plasma mass density, V_φ the *in-situ* measured azimuthal flow velocity, P the total particle pressure, $P_\perp$ the field-perpendicular thermal pressure component, R_C the curvature of the field lines, A the thermal plasma pressure anisotropy ($A=P_\perp/P_\parallel$, $P_\parallel$ being the parallel thermal pressure), J_φ the azimuthal current density and B_z the north-south magnetic field component. The three distinct terms on the left side represent the inertial, the pressure gradient and the pressure anisotropy components of the force per unit volume along the radial direction, and can all be derived from *in-situ* measurements and under the minimal assumptions stated earlier.

The inertial force is directly computed from Cassini/CAPS *in-situ* data (V_φ, ρ, r) and is subsequently fitted as $\log(\rho V_\varphi^2/r)=b_0+b_1r+b_2r^2+b_3r^3+b_4r^4$. The b_i coefficients and are shown in Table 1. The pressure radial gradient is computed by differentiating the polynomial fit to the total particle pressure. The anisotropy force (significant only inside of 8-10 Rs where $P_\perp > P_\parallel$) is directly calculated from the thermal pressure anisotropy measurements available from 6 to 10 R_S [*Wilson et al.,* 2008] and then fitted as $\log(F_A)=c_0+c_1r+c_2r^2$ (coefficients in Table 1). For this range of radial distance the dipole approximation can be safely used to derive the magnetic curvature as $R_C=r/3$. Finally, the vertical component of the magnetic field was also fitted for each LT sector as $\log(B_Z)=d_0+d_1r+d_2r^2+d_3r^3$ (d_i values in Table 1), although the corresponding radial profiles (not presented here) exhibit only weak dependence on local time.

The radial profiles of the three force components are presented in Figure 4 for each LT sector. The pressure gradient force overtakes the inertial force and gradually controls the radial force balance beyond ~9 Rs at all local times. At night, dawn and dusk it stays higher, but on the dayside the two are equal from ~11 to 15 Rs. The distance beyond which the pressure gradient force becomes larger than the inertial force, varies between ~7.5 and 9 Rs.

Inside of 6.5-7 Rs and with decreasing radial distance, the pressure gradient term drops and the inertial force starts to dominate due to higher mass density, despite the increasing opposed anisotropy force. For example, at a radial distance of 6 Rs, the inertial force is well above (at least factor of 4) the pressure gradient and the anisotropy contributions, with the exception of the dayside where the inertial and anisotropy forces are comparable.

As Cassini's instrumentation provides direct measurements of the magnetic field and the (thermal and hot) particle properties along its trajectory, equation (1) can be used to deduce the azimuthal current density J_φ. Solved for J_φ, equation (1) becomes:

$$J_\phi \approx \frac{1}{B_z}\left(\rho\frac{V_\phi^2}{r} - \frac{\partial P}{\partial r} - \frac{P_\perp}{R_C}\left(\frac{A-1}{A}\right)\right) \tag{2}$$

In analogy to equation (1), the three separate terms in the right side of equation (2) correspond to the inertial, pressure gradient, and anisotropy component of the azimuthal current. As mentioned earlier, each of these three terms can be independently determined based on *in-situ*, long term Cassini measurements. The radial profile of the azimuthal current density (pA/m^2) for each LT sector is presented in Figure 5. Due to the complexity and the strong temporal variability of the system, imposed primarily by the hot plasma, the uncertainty in the azimuthal current values can only be roughly estimated, rather than precisely calculated, at ~50%. This ±50% envelope is shown in dotted lines of the same color for each radial profile. A region of maximum J_φ, imposed by the pressure gradient, is observed for the day, dusk and night sectors between ~7 and ~11 Rs. In the dawn sector, the maximum is broader and shifted somewhat outwards (~9 to ~13 Rs). A clear local time asymmetry is also present. At dusk and night sectors the maximum current density, observed at 7.5 Rs and 8.5 Rs respectively, reaches 100-115 pA/m^2. At the dawn sector the broader maximum is considerably lower (60 pA/m^2 at 11.5 Rs). At the dayside, the maximum is well defined at 8.5 Rs, but still lower compared to dusk and the night side, with values close to 85 pA/m^2. Beyond its maximum region, for all local times, the ring current density appears to drop with radial distance faster than the 1/r rate assumed by disc models (e.g. *Connerney et al.* [1983], *Bunce et al.* [2007], *Kellett et al.* [2010]) indicated by the dashed magenta line in Figure 5, yet not as rapidly as reported by *Sergis et al.* [2011].

4. Summary and discussion

After more than 12 years of Cassini in orbit around Saturn, certain issues regarding the nature and characteristics of the complex planetary current system remain unresolved.

In the present work we used a broad data set of combined particle and magnetic field measurements covering nearly 10 years, from the beginning of the mission (mid-2004) to the end of 2013, and attempted to examine the average, global distribution of particle properties in the equatorial Saturnian magnetosphere, and in particular the plasma pressure and the azimuthal current. Apart from the geometrical confinement to the equatorial plane (±1 Rs), magnetic field selection criteria were also applied to the data selection, in order to ensure that only the central plasma sheet environment is sampled.

In agreement with *Sergis et al.* [2007, 2009], but based on a much broader data set, the results show that the particle pressure is controlled by thermal plasma inside of ~8 Rs where the plasma is denser and energetic ion loss due to charge exchange is substantial, and by the hot plasma beyond ~12 Rs. The exact distance of reversal, however, depends on local time, being closer for the dusk and night LT sectors, and farther out for the dawn and dayside. The total particle pressure drops more gradually with radial distance, compared to the thermal plasma pressure profile reported by *Thomsen et al.* [2010], in which, however, there was no LT separation. The measured pressure is also dependent on local time, being higher (factor of ~1.5) on the dusk and on the night side. This local time asymmetry is imposed mainly by the hot plasma pressure component, as ion and ENA measurements in keV energies have indicated in the past.

With almost full particle energy coverage offered by the synergy between the CAPS and MIMI sensors, the total plasma beta was computed. The results verify that the middle and outer Saturnian magnetosphere is characterized by a high plasma beta (>1 beyond 8-10 Rs). Compared to the partial (E<45 keV) plasma beta reported by *Thomsen et al.* [2010], the total plasma beta computed in this study is generally higher by a factor of ~2 and does not drop with radial distance in the middle and outer magnetosphere; both features expected after the inclusion of the hot plasma. Its distribution in local time (not available in previous studies) shows a clear day-night asymmetry with beta values being lower (factor of 2) in the dayside compared to all other LT sectors.

The measurements also allow the separate computation of each force term in the steady state, radial force balance equation (i.e. inertial, pressure gradient, anisotropy) and, hence, the direct computation of the azimuthal current density (see equations 1 and 2). More importantly, we can now determine the relative contribution of each term, provide guidance for models regarding associated physical mechanisms, and examine how the nature of the Saturnian ring current changes with radial distance and local time in the equatorial plasma sheet.

In order to obtain a global view of the ring current and its distribution, we interpolate between the computed current density values, and consequently smooth between the 3-hr wide LT bins, using 1 Rs bins for radial distance as in the radial profiles presented earlier.

The resulting distributions are shown in Figure 6, in the form of color-coded contour maps. Panel (6a) presents the distribution of the ring current density (pA/m^2) in the center of the Saturnian plasma sheet. The average ring current appears as an asymmetric structure, quite similar to what averaged ENA emissions have revealed [*Krimigis et al.,* 2007*; Carbary et al.,* 2008b]. Its maximum region spans from post noon to post midnight (1400-0200 hr) and between 7 and 11 Rs. This picture is consistent with the simulated J_φ distribution produced by global MHD modeling [*Jia et al.,* 2012a], where a broad maximum of ~100 pA/m^2 forms between 10 and 15 Rs (shifted somewhat outwards compared to the results of this study), and remains fixed -although variable- in the night side (from ~1800 to ~0600 hr) throughout the planetary rotation. The displacement of the maximum J_φ region in the simulation could be due to the underestimation of the contribution of the hot plasma pressure for r>10 Rs that largely controls the azimuthal current density. In both cases, nevertheless, the radial profile of the ring current differs from the monotonic 1/r decrease, often adopted in the past.

Panel (6b) illustrates the changing nature of the ring current with radial distance and local time. The color scale parameterizes the relative contributions of the inertial and the pressure gradient components to the total ring current. Red colors correspond to full dominance by the pressure gradient current, whereas blue colors correspond to full dominance by the inertial term. As discussed earlier, the predominant dependence is clearly along the radial distance. There is, however, an obvious local time asymmetry of the driving mechanism of the ring current that, although indicated by ENA imaging and predicted by certain models (e.g. *Jia et al.* [2012a, 2012b]), was not revealed explicitly by *in-situ* data until now. From local afternoon (1600 hr) throughout the night side to local morning (0800 hr), the ring current is inertial inside of 7 Rs (blue color, >70% contribution by the inertial current), pressure gradient driven beyond 11 Rs (yellow and orange, >70% contribution by the pressure-grad current), and displays a mixed nature in the transition zone in-between where its maximum resides (green colors, 40-60% contribution for each current component). On the dayside, however, and in particular for a large sector around local noon (0800-1600 hr), the azimuthal current appears mixed (both inertial and pressure gradient driven) beyond 7 Rs. The maximum of the current density appears essentially unaffected by the anisotropy term.

Note that a less prominent asymmetry is also seen between dawn and dusk; the dawn ring current appears more pressure gradient driven compared to dusk, especially outside of 12 Rs. This feature, as well as the outwards shifted current maximum, are indicative of fast return plasma flow, that has been reproduced by MHD simulations [*Jia et al.,* 2012b] but also observed as a result of (at times impulsive) reconnection of closed field lines in the magnetotail [*Masters et al.,* 2011], consistent with the so-called Vasyliunas cycle [*Vasyliunas,* 1983]. *Thomsen et al.* [2015], presented observational evidence from a non-equatorial Cassini pass, supported also by an MHD simulation, for the formation of a "plasmapause" (i.e. a sharp boundary separating flux tubes that were involved in tail reconnection from those that revolved through the night side without significant mass loss) in the dawn LT sector. The return flow was found to consist of supercorotational, low-density, high-temperature plasma, with significant O+ (magnetospheric) ion content, suggestive of the Vasyliunas cycle. The plasmapause boundary was observed at L=8.6 (i.e. well inside the ring current region). As the return flow channel transfers low density, high temperature magnetospheric plasma, it produces an azimuthal current driven by the hot plasma pressure rather than inertia, for radial distances beyond the location of the -unstable to centrifugally driven interchange- plasmapause, which hence becomes a variable boundary, separating inertial from pressure driven current regimes. The outer limit of our sampling (15 Rs), makes it quite difficult to observe an analogous Dungey-cycle return flow [*Dungey,* 1961], as this would be located farther out [*Badman et al.,* 2007], although the *Thomsen et al.* [2015] reported evidence of Dungey-type lobe reconnection pursuant to the Vasyliunas-type flow pattern. We should note, however, that results concerning the dawn sector should be evaluated with caution, as this LT sector is not yet sampled adequately. It becomes also evident from the map of Figure 5, that, at least for certain LT sectors (e.g. dusk and night side), the ring current is strongly affected by the particle pressure (i.e. a maximum J_φ region forms), even during times of moderate magnetospheric activity.

The ring current constitutes an essential part of the magnetospheric current system and the global magnetospheric-ionospheric coupling. Its divergence is closely related to the structure and strength of the field-aligned currents (see theoretical analysis by *Vasyliunas*, 1984) that are responsible for the coupling between the magnetosphere and ionosphere conveying angular momentum from the planet to its surrounding plasma disc in an attempt to maintain rigid corotation between the two regions.

In addition, the magnetosphere-ionosphere coupling at Saturn strongly affects (and perhaps drives) the observed, but not yet fully understood, periodicities in several magnetospheric phenomena, varying with a period very close to the planetary rotation [*Carbary and Mitchell,* 2013]. As data from the Cassini Radio and Plasma Wave Science Instrument (RPWS) have confirmed, the period of the Saturnian radio emission changes slowly, indicating that the source of the observed periodicities must be related to a complex and asymmetric atmosphere-ionosphere-magnetosphere coupling, rather than the interior of the planet. Therefore, the detailed mapping of the ring current and the study of the interacting current components (radial and field-aligned) that constitute the three-dimensional magnetospheric current system, become important in many aspects. The "proximal" orbit phase of Cassini (September 2017) will provide a unique opportunity to obtain measurements on the high-latitude magnetosphere very close to the planet, and bring us closer to forming a more complete picture of the Saturnian current system.

A long-standing question regarding the structure and the nature of the Saturnian ring current (and global current system in general) has always been whether it is more "Earth-like" or "Jupiter-like". Although both Saturn and Earth possess well-observed ring currents, these azimuthal charged particle flows cannot easily be viewed as analogues to each other. The Satunian ring current is significantly modulated by the fast planetary rotation, well protected from the solar wind, and supplied by ions mainly from an internal source (Enceladus). In Earth's case, ground and spacecraft measurements have shown that during "quiet" times the symmetric ring current is relatively weak and carried mostly by solar wind particles, intensifying during magnetic storms with a simultaneous change in its composition (i.e. becoming O+ dominated). These fundamental differences make any detailed comparison between the Saturnian and the Terrestrial ring current quite hard to attempt (see also discuss by *Kivelson* [2005]). On the other hand, with a major plasma source located close to the planet and embedded in a rotational-dominated, semi-permanent plasmadisc, the Saturnian ring current has much more in common with the current flow in Jupiter's middle magnetosphere.

Despite their similarities, the two giant magnetospheres seem to have differences, sometimes less obvious, that also reflect to their azimuthal currents. As an example, *Vasyliunas* [2008] described how the relative mass input is most likely larger at Saturn than at Jupiter, as certain scale quantities, such as the solar wind mass flux on the projected magnetospheric area or the mass flux required to completely prevent corotation, are much smaller at Saturn compared to Jupiter. Even though a detailed comparison between the two azimuthal currents is beyond the scope of this study, we should note that, based on its greater effect on the planetary magnetic field, the Saturnian ring current could be considered stronger than the Jovian one, although weaker when measured in absolute values.

Acknowledgments

We are grateful to MIMI team colleagues for comments that improved this study. We thank M. Kusterer and J. Vandegriff (JHU/APL) for assistance with the MIMI data. Work at JHU/APL was supported by NASA and by subcontracts at the University of Maryland and the Academy of Athens. Work at PSI was supported by the NASA/Cassini program through JPL contract 1243218 with Southwest Research Institute. C.M.J. is supported by a Science and Technology Facilities Council Ernest Rutherford Fellowship number ST/L004399/1. The data used in this study can be found in files online at the NASA Planetary Data System (PDS) at http://pds.nasa.gov.

References

Achilleos, N., P. Guio, C. S. Arridge, N. Sergis, R. J. Wilson, M. F. Thomsen, and A. J. Coates (2010), Influence of hot plasma pressure on the global structure of Saturn's magnetodisk, Geophys. Res. Lett., 37, L20201, doi:10.1029/2010GL045159.

Arridge, C. S., K. K. Khurana, C. T. Russell, D. J. Southwood, N. Achilleos, M. K. Dougherty, A. J. Coates, and H. K. Leinweber (2008), Warping of Saturn's magnetospheric and magnetotail current sheets, J. Geophys. Res., 113, A08217, doi:10.1029/2007JA012963.

Arridge, C. S., et al. (2011), Periodic motion of Saturn's nightside plasma sheet, J. Geophys. Res., 116, A11205, doi:10.1029/2011JA016827.

Badman, S. V., and S. W. H. Cowley (2007), Significance of Dungey‐ cycle flows in Jupiter's and Saturn's magnetospheres, and their identifi- cation on closed equatorial field lines, Ann. Geophys., 25, 941–951, doi:10.5194/angeo-25-941-2007.

Brandt, P.C., K.K. Khurana, D.G. Mitchell, N. Sergis, K. Dialynas, J.F. Carbary, E.C. Roelof, C.P. Paranicas, S.M. Krimigis, and B.H. Mauk (2010), Saturn's periodic magnetic field perturbations caused by a rotating partial ring current, *Geophys. Res. Lett., 37,* L22103, doi:10.1029/2010GL045285.

Bunce, E. J., and S. W. H. Cowley (2003), A note on the ring current in Saturn's magnetosphere: Comparison of magnetic data obtained during the Pioneer-11 and Voyager-1 and -2 fly-bys, Ann. Geophys., 21, 661– 669.

Bunce, E. J. et al., (2007), Cassini observations of the variation of Saturn's ring current parameters with system size, *J. Geophys. Res., 112,* A10, CiteID A10202, doi: 10.1029/2007JA012275.

Burch, J. L., J. Goldstein, T. W. Hill, D. T. Young, F. J. Crary, A. J. Coates, N. André, W. S. Kurth, and E. C. Sittler Jr. (2005), Properties of local plasma injections in Saturn's magnetosphere, Geophys. Res. Lett., 32, L14S02, doi:10.1029/2005GL022611.

Carbary, J. F., D. G. Mitchell, C. Paranicas, E. C. Roelof, and S. M. Krimigis (2008a), Direct observation of warping in the plasma sheet of Saturn, Geophys. Res. Lett., 35, L24201, doi:10.1029/2008GL035970.

Carbary, J. F., D.G. Mitchell, P. Brandt, E.C. Roelof, and S.M. Krimigis (2008b), Statistical morphology of ENA emissions at Saturn, *J. Geophys. Res., 113,* A05210, doi: 10.1029/2007JA012873.

Carbary, J. F., and D. G. Mitchell (2013), Periodicities in Saturn's magnetosphere, *Rev. Geophys., 51,*1–30, doi: 10.1002/rog.20006.

Chen, Y., and T. W. Hill (2008), Statistical analysis of injection/dispersion events in Saturn's inner magnetosphere, J. Geophys. Res., 113, A07215, doi:10.1029/2008JA013166.

Connerney, J. E. P., M.H. Acuña, and N.F. Ness, (1981), Saturn's ring current and inner magnetosphere, *Nature*, *292*, 724-726.

Connerney, J. E. P., M.H. Acuña and N.F. Ness, (1983), Currents in Saturn's magnetosphere, *J. Geophys. Res., 88,* 8779-8789.

Connerney, J. E. P., Acuña, M. H., and Ness, N. F.: The Z3 model of Saturn's magnetic field and the Pioneer 11 vector helium magnetometer observations, J. Geophys. Res., 89, 7541, 1984.

Davis, Jr., L. and Smith, E. J.: A model of Saturn's magnetic field based on all available data, J. Geophys. Res., 95, 15 257, 1990.

Dougherty, M. K. et al., (2004), The Cassini Magnetic Field Investigation, *Space Sci. Rev.*, Volume 114, Issue 1-4, pp. 331-383, doi: 10.1007/s11214-004-1432-2.

Dungey, J. W. (1961), Interplanetary magnetic field and the auroral zones, Phys. Rev. Lett., 6, 47–48, doi:10.1103/PhysRevLett.6.47.

Hill, T. W., A. M. Rymer, J. L. Burch, F. J. Crary, D. T. Young, M. F. Thomsen, D. Delapp, N. André, A. J. Coates, and G. R. Lewis (2005), Evidence for rotationally driven plasma transport in Saturn's magnetosphere, Geophys. Res. Lett., 32, L14S10, doi:10.1029/2005GL022620.

Jia, X., M. G. Kivelson, and T. I. Gombosi (2012a), Driving Saturn's magnetospheric periodicities from the upper atmosphere/ionosphere, J. Geophys. Res., 117, A04215, doi:10.1029/2011JA017367.

Jia, X., K. C. Hansen, T. I. Gombosi, M. G. Kivelson, G. Tóth, D. L. DeZeeuw, and A. J. Ridley (2012b), Magnetospheric configuration and dynamics of Saturn's magnetosphere: A global MHD simulation, J. Geophys. Res., 117, A05225, doi:10.1029/2012JA017575.

Kellett, S., C. S. Arridge, E. J. Bunce, A. J. Coates, S. W. H. Cowley, M. K. Dougherty, A. M. Persoon, N. Sergis, and R. J. Wilson (2010), Nature of the ring current in Saturn's dayside magnetosphere, J. Geophys. Res., 115, A08201, doi:10.1029/2009JA015146.

Kellett, S., C. S. Arridge, E. J. Bunce, A. J. Coates, S. W. H. Cowley, M. K. Dougherty, A. M. Persoon, N. Sergis, and R. J. Wilson (2011), Saturn's ring current: Local time dependence and temporal variability, J. Geophys. Res., 116, A05220, doi:10.1029/2010JA016216.

Kennelly, T. J., J. S. Leisner, G. B. Hospodarsky, and D. A. Gurnett (2013), Ordering of injection events within Saturnian SLS longitude and local time, J. Geophys. Res. Space Physics, 118, 832–838, doi:10.1002/ jgra.50152.

Kivelson, M. G. (2005), The Current Systems of the Jovian Magnetosphere and Ionosphere and Predictions for Saturn, Space Science Reviews 116: 299–318, doi: 10.1007/s11214-005-1959-x.

Krimigis, S. M. et al. (1981), Low-energy charged particles in Saturn's magnetosphere-Results from Voyager 1, *Science, 212,* 225-231.

Krimigis, S. M., J. F. Carbary, E. P. Keath, T. P. Armstrong, L. J. Lanzerotti, G. Gloeckler, (1983), General characteristics of hot plasma and energetic particles in the Saturnian magnetosphere-Results from the Voyager spacecraft, *J. Geophys. Res., 88,* 8871-8892.

Krimigis, S. M. et al. (2004), Magnetosphere Imaging Instrument (MIMI) on the Cassini Mission to Saturn/Titan, *Space Sci. Rev., 114,* 233-329.

Krimigis, S. M., N. Sergis, D.G. Mitchell, D.C. Hamilton and N. Krupp (2007), A dynamic, rotating ring current around Saturn, *Nature*, Volume 450, Issue 7172, pp. 1050-1053, doi: 10.1038/nature06425.

Krupp, N., et al. (2005), The Saturnian plasma sheet as revealed by energetic particle measurements, Geophys. Res. Lett., 32, L20S03, doi:10.1029/2005GL022829.

Livi, R., J. Goldstein, J. L. Burch, F. Crary, A. M. Rymer, D. G. Mitchell, and A. M. Persoon (2014), Multi-instrument analysis of plasma parameters in Saturn's equatorial, inner magnetosphere using corrections for spacecraft potential and penetrating background radiation, J. Geophys. Res. Space Physics, 119, 3683–3707, doi:10.1002/2013JA019616.

Masters, A., M. F. Thomsen, S. V. Badman, C. S. Arridge, D. T. Young, A. J. Coates, and M. K. Dougherty (2011), Supercorotating return flow from reconnection in Saturn's magnetotail, Geophys. Res. Lett., 38, L03103, doi:10.1029/2010GL046149.

Mauk, B. H., S. M. Krimigis and R.P. Lepping (1985), Particle and field stress balance within a planetary magnetosphere, *J. Geophys. Res., 90,* 8253-8264.

Mauk, B. H. et al., (2005), Energetic particle injections in Saturn's magnetosphere, *Geophys. Res. Lett., 32,* Issue 14, doi: 10.1029/2005GL022485.

Ness, N. F., Acuña, M. H., Lepping, R. P., Connerney, J. E. P., Behannon, K. W., Burlaga, L. F., and Neubauer, F.: Magnetic field studies by Voyager 1: Preliminary results at Saturn, Science, 212, 211, 1981.

Ness, N. F., Acuña M. H., Behannon, K. W., Burlaga, L. F., Connerney, J. E. P., Lepping, R. P., and Neubauer, F.: Magnetic field studies by Voyager 2: Preliminary results at Saturn, Science, 215, 558, 1982.

Paranicas, C. P. et al., (2007), Energetic electrons injected into Saturn's neutral gas cloud, *Geophys. Res. Lett., 34,* Issue 2, CiteID L02109, doi: 10.1029/2006GL028676.

Rymer, A. M., et al. (2009), Cassini evidence for rapid interchange transport at Saturn, Planet. Space. Sci., 57, 1779.

Sergis, N. et al., (2007), Ring current at Saturn: Energetic particle pressure in Saturn's equatorial magnetosphere measured with Cassini/MIMI, *Geophys. Res. Lett., 34,* Issue 9, CiteID L09102, doi: 10.1029/2006GL029223.

Sergis, N. et al., (2009), Energetic particle pressure in Saturn's magnetosphere, measured with Magnetospheric Imaging Instrument on Cassini, *J. Geophys. Res., 114, A2,* CiteID A02214, doi: 10.1029/2008JA013774.

Sergis, N., et al. (2010), Particle pressure, inertial force, and ring current density profiles in the magnetosphere of Saturn, based on Cassini measurements, Geophys. Res. Lett., 37, L02102, doi:10.1029/ 2009GL041920.

Sergis, N., C. S. Arridge, S. M. Krimigis, D. G. Mitchell, A. M. Rymer, D. C. Hamilton, N. Krupp, M. K. Dougherty, and A. J. Coates (2011), Dynamics and seasonal variations in Saturn's magnetospheric plasma sheet, as measured by Cassini, J. Geophys. Res., 116, A04203, doi:10.1029/2010JA016180.

Sittler, E. C. et al., (2008), Ion and neutral sources and sinks within Saturn's inner magnetosphere: Cassini results, *Planet Space Sci., 56,*doi: 10.1016/j.pss.2007.06.006.

Thomsen, M. F., D. B. Reisenfeld, D. M. Delapp, R. L. Tokar, D. T. Young, F. J. Crary, E. C. Sittler, M. A. McGraw, and J. D. Williams (2010), Survey of ion plasma parameters in Saturn's magnetosphere, J. Geophys. Res., 115, A10220, doi: 10.1029/2010JA015267.

Thomsen, M. F. (2013), Saturn's magnetospheric dynamics, Geophys. Res. Lett., 40, 5337–5344, doi:10.1002/2013GL057967.

Thomsen, M. F., et al. (2014), Ion composition in interchange injection events in Saturn's magnetosphere, J. Geophys. Res. Sp ace Physics, 119, 9761–9772, doi: 10.1002/2014JA020489.

Thomsen, M. F., D. G. Mitchell, X. Jia, C. M. Jackman, G. Hospodarsky, and A. J. Coates (2015), Plasmapause formation at Saturn, J. Geophys. Res. Space Physics, 120, 2571–2583, doi:10.1002/2015JA021008.

Vasyliunas, V. M. (1983), Plasma distribution and flow, in Physics of the Jovian Magnetosphere, edited by A. J. Dessler, chap. 11, pp. 395–453, Cambridge Univ. Press, New York.

Vasyliunas, V. M. (1984), Fundamentals of current description, in Magnetospheric Currents, Geophys. Monogr. Ser., vol. 28, edited by T. A. Potemra, pp. 63–66, AGU, Washington, D. C.

Vasyliunas, V. M. (2008), Comparing Jupiter and Saturn: dimensionless input rates from plasma sources within the magnetosphere, Ann. Geophys., 26, 1341–1343.

Wilson, R. J., R. L. Tokar, M. G. Henderson, T. W. Hill, M. F. Thomsen, D. H. Pontius Jr., (2008), Cassini Plasma Spectrometer Thermal Ion Measurements in Saturn's Inner Magnetosphere, *J. Geophys. Res., 113,* CiteID A112218, doi: 10.1029/2008JA013486

Young, D.T. et al., (2004), Cassini Plasma Spectrometer Investigation, *Space Sci. Rev.*, *114*, Issue 1-4, pp. 1-112, doi: 10.1007/s11214-004-1406-4.

Table 1.

	NIGHT	DAWN	DAY	DUSK
P (Pa)	a_0=-1.082×10^{1}	a_0=-9.134×10^{0}	a_0=-1.796×10^{1}	a_0=-1.080×10^{1}
	a_1=+8.399×10^{-1}	a_1=-1.622×10^{-1}	a_1=+3.730×10^{0}	a_1=+6.899×10^{-1}
	a_2=-1.471×10^{-1}	a_2=+2.623×10^{-2}	a_2=-5.697×10^{-1}	a_2=-1.023×10^{-1}
	a_3=+9.470×10^{-3}	a_3=-2.360×10^{-3}	a_3=+3.530×10^{-2}	a_3=+5.200×10^{-3}
	a_4=-2.165×10^{-4}	a_4=+6.594×10^{-5}	a_4=-7.795×10^{-4}	a_4=-8.675×10^{-5}
$\frac{\boldsymbol{\rho V_\varphi^2}}{\mathbf{r}}$ (N/m^3)	b_0=-2.488×10^{1}	b_0=-1.880×10^{1}	b_0=-2.127×10^{1}	b_0=-2.101×10^{1}
	b_1=+3.844×10^{0}	b_1=+1.106×10^{0}	b_1=+1.782×10^{0}	b_1=+1.811×10^{0}
	b_2=-6.441×10^{-1}	b_2=-2.456×10^{-1}	b_2=-2.837×10^{-1}	b_2=-2.779×10^{-1}
	b_3=+4.193×10^{-2}	b_3=+1.904×10^{-2}	b_3=+1.708×10^{-2}	b_3=+1.504×10^{-2}
	b_4=-9.593×10^{-4}	b_4=-5.320×10^{-4}	b_4=-3.675×10^{-4}	b_4=-2.719×10^{-4}
$\mathbf{F_A}$ (N/m^3)	c_0=-1.278×10^{1}	c_0=-1.798×10^{1}	c_0=-1.542×10^{1}	c_0=-1.626×10^{1}
	c_1=-1.088×10^{0}	c_1=-8.900×10^{-2}	c_1=-4.159×10^{-1}	c_1=-2.300×10^{-1}
	c_2=+4.974×10^{-2}	c_2=+3.380×10^{-3}	c_2=+8.230×10^{-3}	c_2=-4.540×10^{-3}
$\mathbf{B_Z}$ (nT)	d_0=+4.304×10^{0}	d_0=+4.304×10^{0}	d_0=+4.338×10^{0}	d_0=+4.513×10^{0}
	d_1=-5.475×10^{-1}	d_1=-5.530×10^{-1}	d_1=-5.568×10^{-1}	d_1=-5.988×10^{-1}
	d_2=+2.727×10^{-2}	d_2=+2.804×10^{-2}	d_2=+2.860×10^{-2}	d_2=+3.131×10^{-2}
	d_3=-4.818×10^{-4}	d_3=-4.758×10^{-4}	d_3=-5.052×10^{-4}	d_3=-5.665×10^{-4}
$\mathbf{J_\varphi}$ (pA/m^2)	e_0=-1.782×10^{1}	e_0=-9.102×10^{0}	e_0=-4.443×10^{1}	e_0=-1.646×10^{1}
	e_1=+3.042×10^{0}	e_1=-5.560×10^{-1}	e_1=+1.292×10^{1}	e_1=+2.264×10^{0}
	e_2=-4.300×10^{-1}	e_2=+7.781×10^{-2}	e_2=-1.792×10^{0}	e_2=-2.874×10^{-1}
	e_3=+2.631×10^{-2}	e_3=-3.850×10^{-3}	e_3=+1.092×10^{-1}	e_3=+1.599×10^{-2}
	e_4=-5.797×10^{-4}	e_4=+4.736×10^{-5}	e_4=-2.490×10^{-3}	e_4=-3.437×10^{-4}

Table 1. Coefficients of the polynomial fit functions (see text) describing Saturn's magnetospheric properties as a function of radial distance r, for each LT sector.

Figure captions

Figure 1. Statistical distribution in radial distance (upper panel) and local time (lower panel) of the data used in the present study. Magnetic field and hot plasma sampling statistics are shown in black columns (labeled MAG and MIMI), the thermal plasma coverage is shown in gray columns (labeled CAPS).

Figure 2. Average radial pressure profile for thermal ion plasma (black squares), energetic particles (red dots) and total (blue triangles) for four 6-hr wide LT sectors, indicated within each panel. The error bars correspond to the standard error of the mean for each bin.

Figure 3. Average radial profile of the total plasma beta for four 6-hr wide LT sectors in the Saturnian magnetosphere, centered at midnight (0000 hr), dawn (0600 hr), noon (1200) and dusk (1800). The error bars correspond to the standard error of the mean for each bin.

Figure 4. Average radial profiles (polynomial fits) of the inertial body force (blue), the particle pressure gradient force (red) and the pressure anisotropy force (black) for four 6-hr wide LT sectors in the Saturnian magnetosphere, centered at midnight (0000 hr), dawn (0600 hr), noon (1200) and dusk (1800). The corresponding functions and coefficients can be found in text and in Table 1, respectively.

Figure 5. Average radial profiles (polynomial fits) of the total ring current density J_φ for four 6-hr wide LT sectors in the Saturnian magnetosphere, centered at midnight (0000 hr), dawn (0600 hr), noon (1200) and dusk (1800). Dotted curves of the same color for each radial profile bracket a ± 50% envelope, as the estimated uncertainty in J_φ due to the intense dynamics of the Saturnian ring current. The dashed magenta line represents a 1/r decrease.

Figure 6. (a): Contour map illustrating the average distribution of the average azimuthal current, and its dependence on radial distance and local time in the equatorial magnetosphere of Saturn. Dashed circles indicate radial distances of 5, 10 and 15 Rs. The color scale describes the current density in pA/m^2. **(b):** Similar to (a), map demonstrating the nature of the average Saturnian ring current. The color scale shows the contribution of the pressure gradient driven current ($-\frac{1}{B_z}\frac{\partial P}{\partial r}$) to the total measured current. Dashed circles indicate radial distances of 5, 10 and 15 Rs. The Sun in both representations is to the left.

Table 1.

Polynomial fit coefficients for Saturn's magnetospheric properties				
	NIGHT	**DAWN**	**DAY**	**DUSK**
P (Pa)	a_0=-1.082×10^{1} a_1=+8.399×10^{-1} a_2=-1.471×10^{-1} a_3=+9.470×10^{-3} a_4=-2.165×10^{-4}	a_0=-9.134×10^{0} a_1=-1.622×10^{-1} a_2=+2.623×10^{-2} a_3=-2.360×10^{-3} a_4=+6.594×10^{-5}	a_0=-1.796×10^{1} a_1=+3.730×10^{0} a_2=-5.697×10^{-1} a_3=+3.530×10^{-2} a_4=-7.795×10^{-4}	a_0=-1.080×10^{1} a_1=+6.899×10^{-1} a_2=-1.023×10^{-1} a_3=+5.200×10^{-3} a_4=-8.675×10^{-5}
$\frac{\boldsymbol{\rho V_\varphi^2}}{\mathbf{r}}$ (N/m^3)	b_0=-2.488×10^{1} b_1=+3.844×10^{0} b_2=-6.441×10^{-1} b_3=+4.193×10^{-2} b_4=-9.593×10^{-4}	b_0=-1.880×10^{1} b_1=+1.106×10^{0} b_2=-2.456×10^{-1} b_3=+1.904×10^{-2} b_4=-5.320×10^{-4}	b_0=-2.127×10^{1} b_1=+1.782×10^{0} b_2=-2.837×10^{-1} b_3=+1.708×10^{-2} b_4=-3.675×10^{-4}	b_0=-2.101×10^{1} b_1=+1.811×10^{0} b_2=-2.779×10^{-1} b_3=+1.504×10^{-2} b_4=-2.719×10^{-4}
$\mathbf{F_A}$ (N/m^3)	c_0=-1.278×10^{1} c_1=-1.088×10^{0} c_2=+4.974×10^{-2}	c_0=-1.798×10^{1} c_1=-8.900×10^{-2} c_2=+3.380×10^{-3}	c_0=-1.542×10^{1} c_1=-4.159×10^{-1} c_2=+8.230×10^{-3}	c_0=-1.626×10^{1} c_1=-2.300×10^{-1} c_2=-4.540×10^{-3}
$\mathbf{B_Z}$ (nT)	d_0=+4.304×10^{0} d_1=-5.475×10^{-1} d_2=+2.727×10^{-2} d_3=-4.818×10^{-4}	d_0=+4.304×10^{0} d_1=-5.530×10^{-1} d_2=+2.804×10^{-2} d_3=-4.758×10^{-4}	d_0=+4.338×10^{0} d_1=-5.568×10^{-1} d_2=+2.860×10^{-2} d_3=-5.052×10^{-4}	d_0=+4.513×10^{0} d_1=-5.988×10^{-1} d_2=+3.131×10^{-2} d_3=-5.665×10^{-4}
$\mathbf{J_\varphi}$ (pA/m^2)	e_0=-1.782×10^{1} e_1=+3.042×10^{0} e_2=-4.300×10^{-1} e_3=+2.631×10^{-2} e_4=-5.797×10^{-4}	e_0=-9.102×10^{0} e_1=-5.560×10^{-1} e_2=+7.781×10^{-2} e_3=-3.850×10^{-3} e_4=+4.736×10^{-5}	e_0=-4.443×10^{1} e_1=+1.292×10^{1} e_2=-1.792×10^{0} e_3=+1.092×10^{-1} e_4=-2.490×10^{-3}	e_0=-1.646×10^{1} e_1=+2.264×10^{0} e_2=-2.874×10^{-1} e_3=+1.599×10^{-2} e_4=-3.437×10^{-4}

Figure 1.

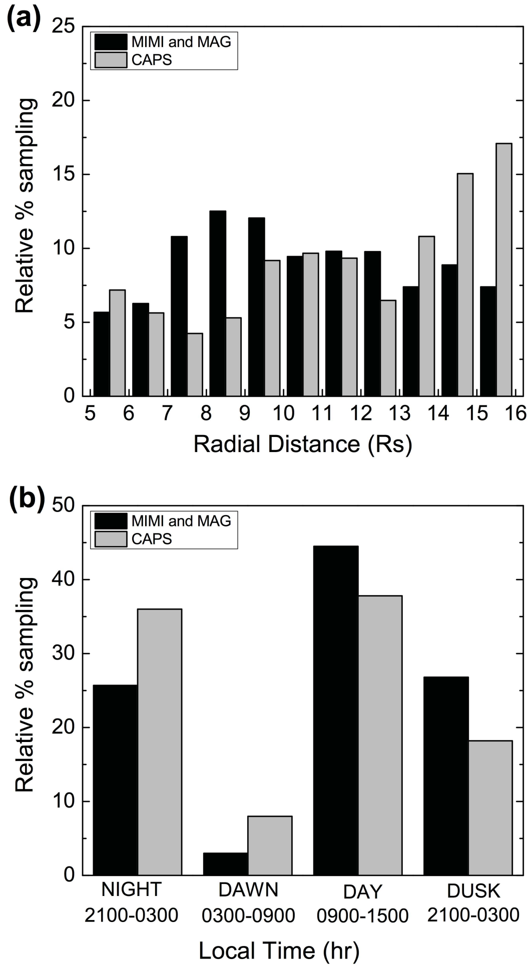
(a)
MIMI and MAG
CAPS
Relative % sampling
Radial Distance (Rs)
(b)
MIMI and MAG
CAPS
Relative % sampling
NIGHT 2100-0300
DAWN 0300-0900
DAY 0900-1500
DUSK 2100-0300
Local Time (hr)

Figure 2.

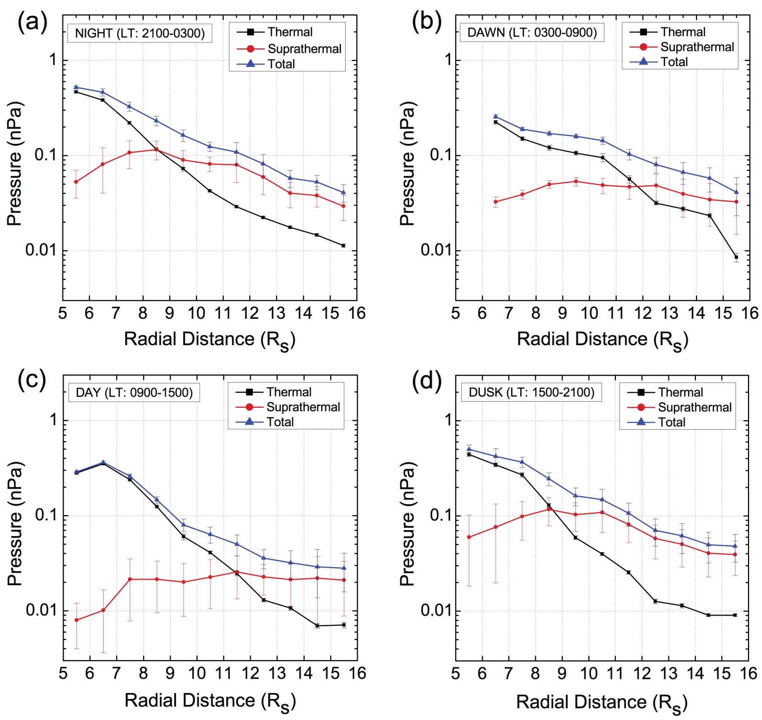
(a)
NIGHT (LT: 2100-0300)
Thermal
Suprathermal
Total
Pressure (nPa)
Radial Distance (R_S)
(b)
DAWN (LT: 0300-0900)
Thermal
Suprathermal
Total
Pressure (nPa)
Radial Distance (R_S)
(c)
DAY (LT: 0900-1500)
Thermal
Suprathermal
Total
Pressure (nPa)
Radial Distance (R_S)
(d)
DUSK (LT: 1500-2100)
Thermal
Suprathermal
Total
Pressure (nPa)
Radial Distance (R_S)

Figure 3.

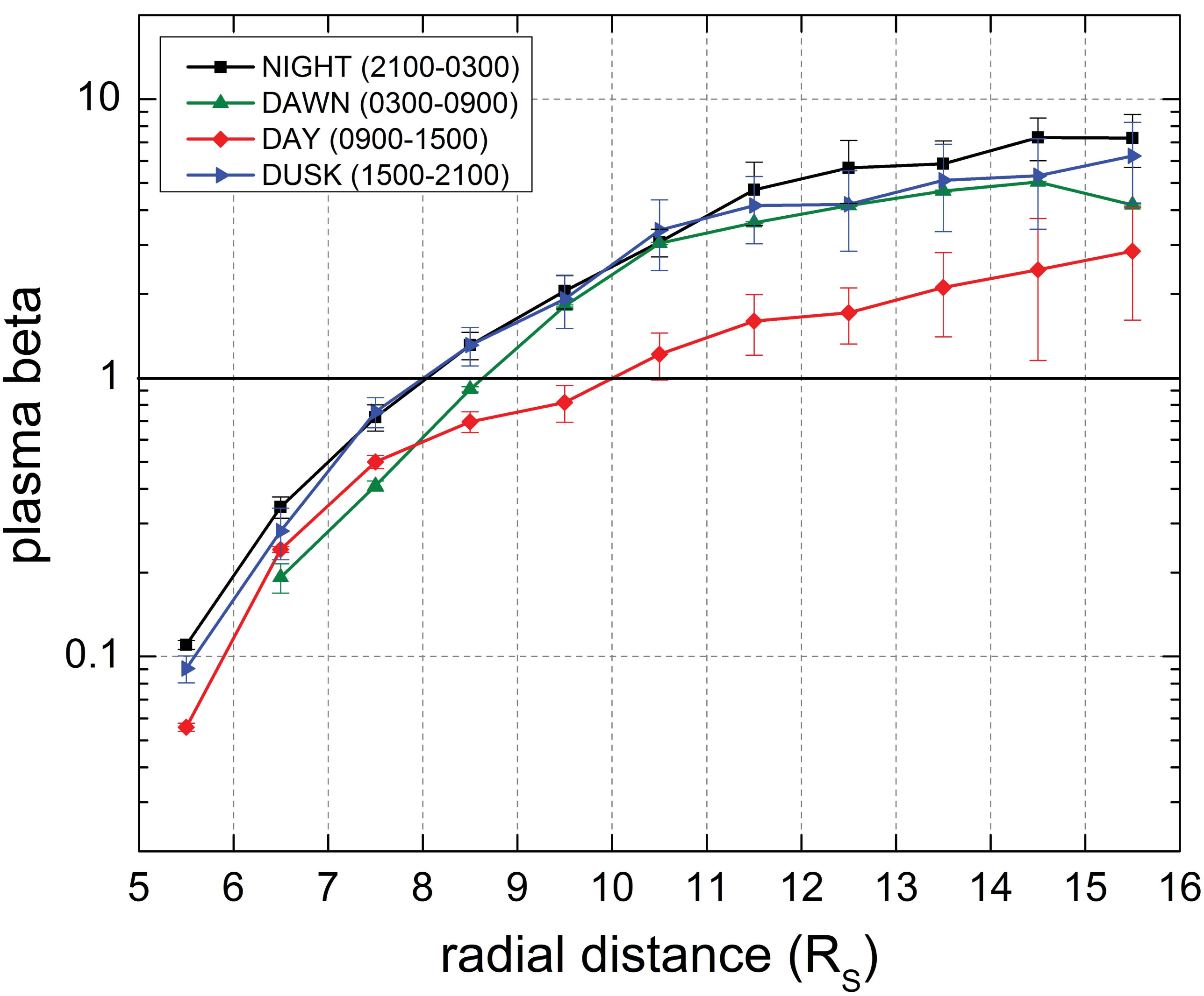
NIGHT (2100-0300)
DAWN (0300-0900)
DAY (0900-1500)
DUSK (1500-2100)
plasma beta
10
1
0.1
5
6
7
8
9
10
11
12
13
14
15
16
radial distance (R_S)

Figure 4.

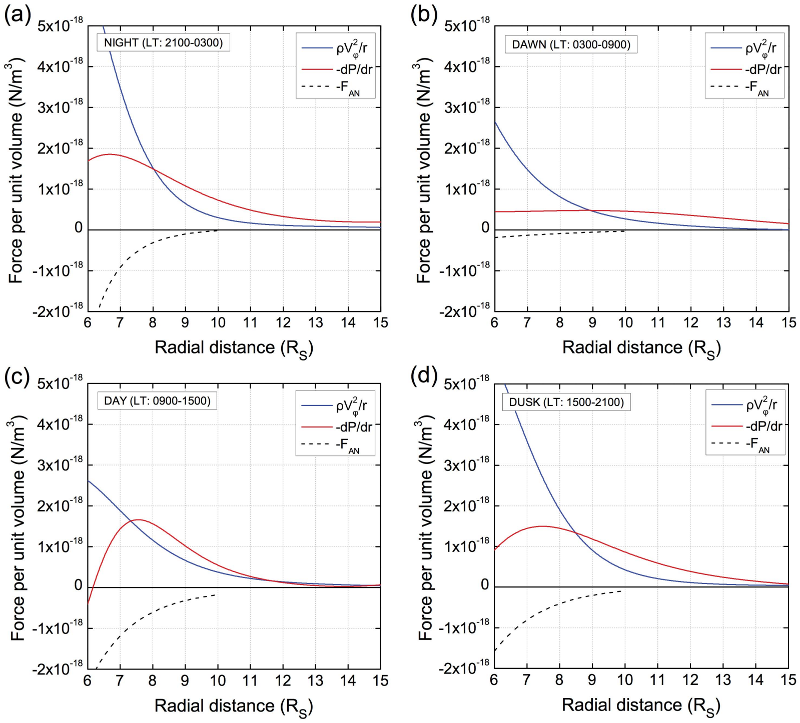

(a)
NIGHT (LT: 2100-0300)
(b)
DAWN (LT: 0300-0900)
(c)
DAY (LT: 0900-1500)
(d)
DUSK (LT: 1500-2100)
$\rho V_\varphi^2/r$
$-dP/dr$
$-F_{AN}$
Force per unit volume (N/m^3)
Radial distance (R_S)
5×10^{-18}
4×10^{-18}
3×10^{-18}
2×10^{-18}
1×10^{-18}
0
-1×10^{-18}
-2×10^{-18}
6 7 8 9 10 11 12 13 14 15

Figure 5.

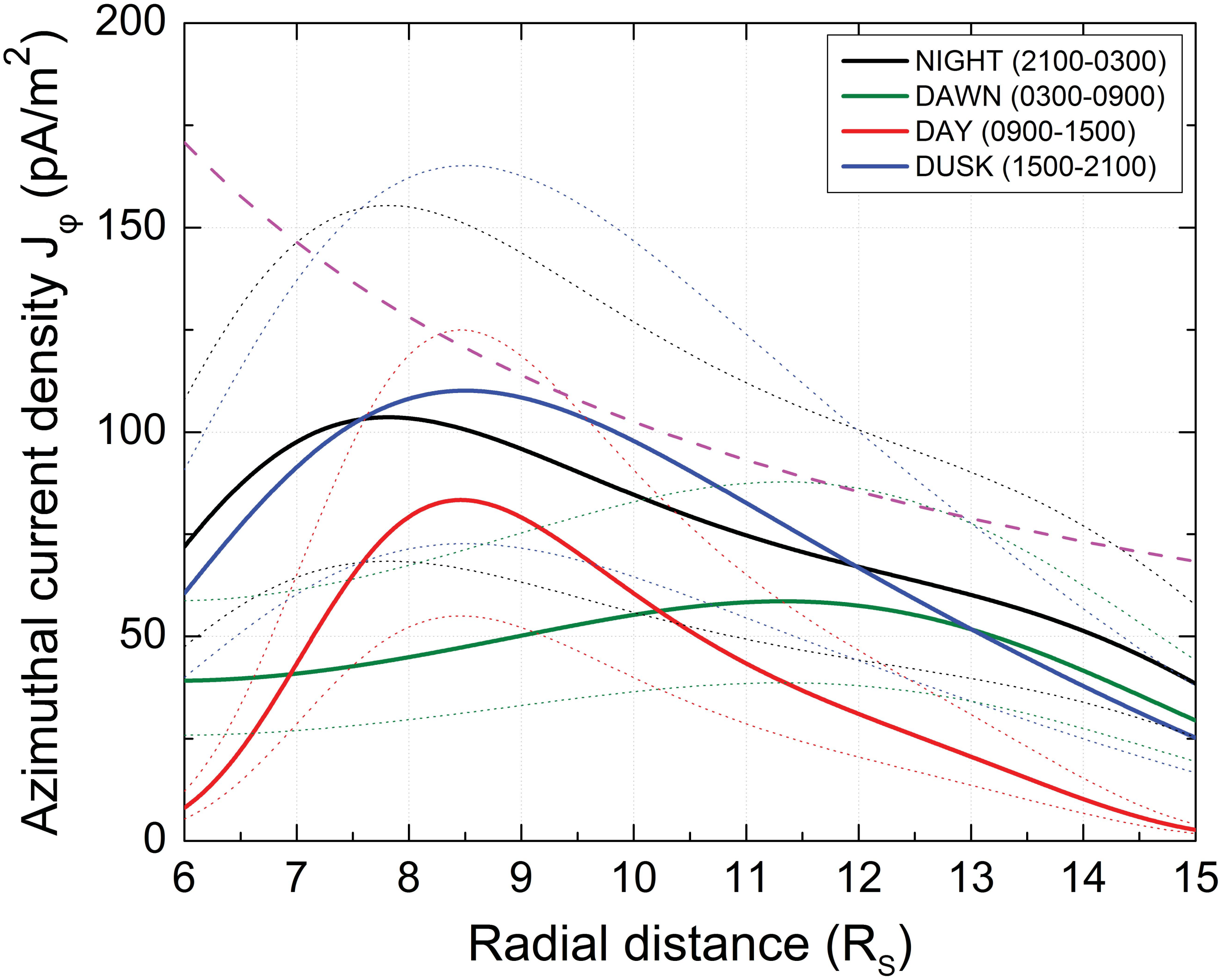

NIGHT (2100-0300)
DAWN (0300-0900)
DAY (0900-1500)
DUSK (1500-2100)
Azimuthal current density J_φ (pA/m^2)
Radial distance (R_S)
0
50
100
150
200
6
7
8
9
10
11
12
13
14
15

Figure 6.

(a)

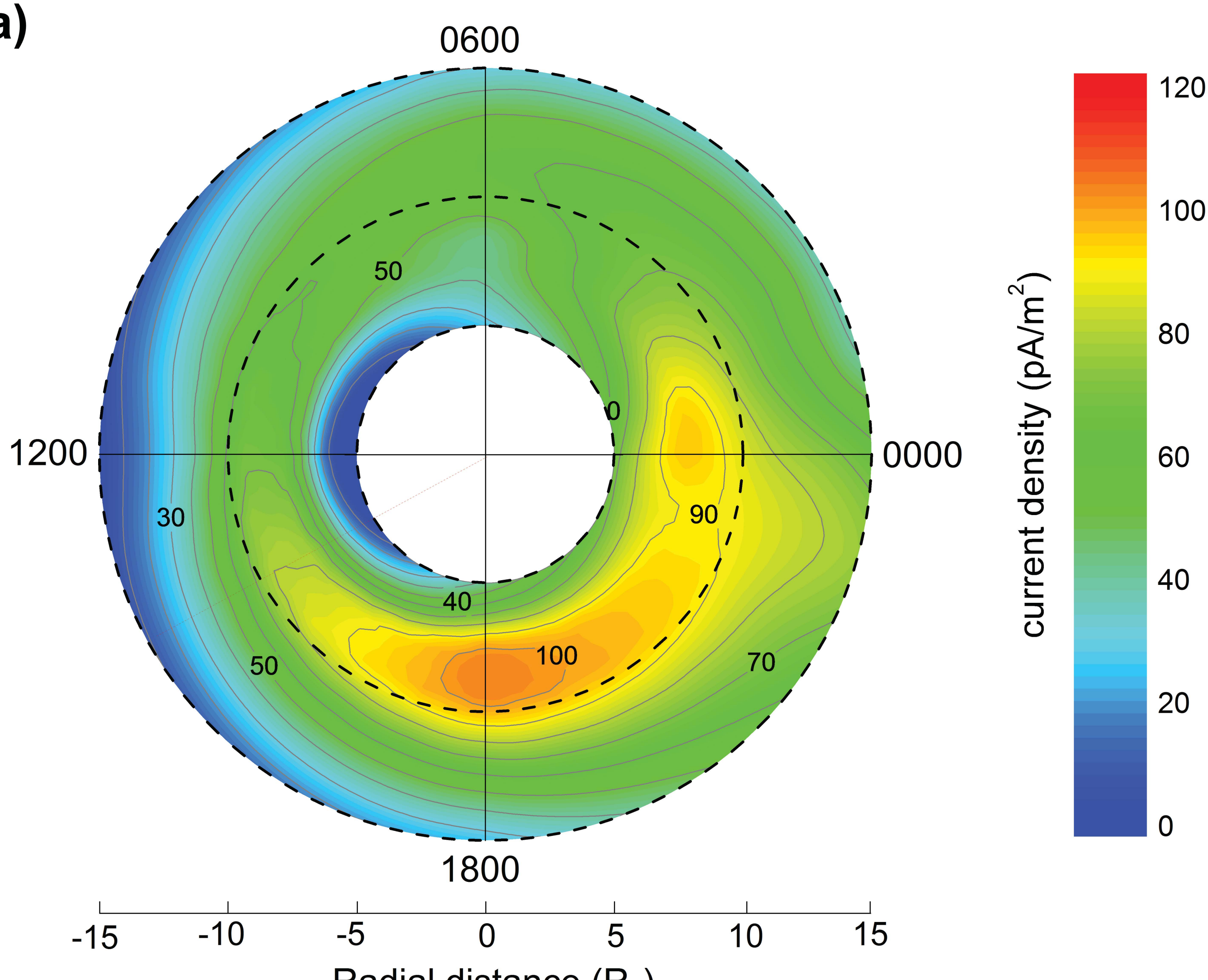

0600
1200
0000
1800
50
0
90
30
40
100
50
70
-15
-10
-5
0
5
10
15
Radial distance (R_s)
120
100
80
60
40
20
0
current density (pA/m^2)

Figure 7.

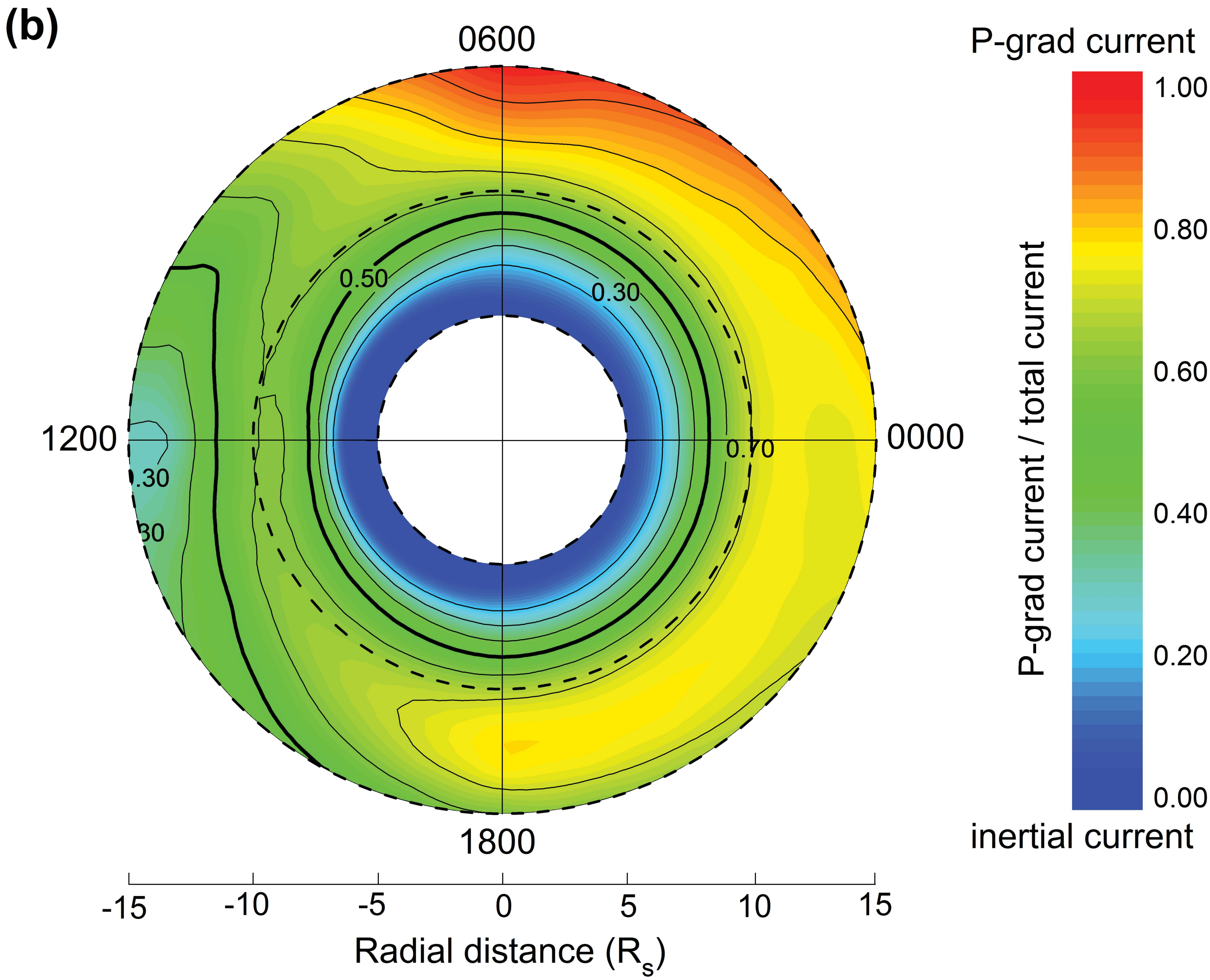

(b)
0600
1200
0000
1800
0.50
0.30
0.70
.30
30
-15
-10
-5
0
5
10
15
Radial distance (R_s)
P-grad current
1.00
0.80
0.60
0.40
0.20
0.00
P-grad current / total current
inertial current